# Distinguishing dynamics using recurrence-time statistics

E. J. Ngamga,[1] D. V. Senthilkumar,[1] A. Prasad,[2] P. Parmananda,[3] N. Marwan,[1] and J. Kurths[1,4,5]
[1]*Potsdam Institute for Climate Impact Research, Telegraphenberg A 31, 14473 Potsdam, Germany*
[2]*Department of Physics and Astrophysics, University of Delhi, Delhi 110007, India*
[3]*Department of Physics, Indian Institute of Technology Bombay, Powai 400076, Maharashtra, India*
[4]*Department of Physics, Humboldt University Berlin, 12489 Berlin, Germany*
[5]*Institute for Complex Systems and Mathematical Biology, University of Aberdeen, Aberdeen AB24 3UE, United Kingdom*
(Received 20 October 2010; revised manuscript received 15 December 2011; published 27 February 2012)

The probability densities of the mean recurrence time, which is the average time needed for a system to recur to a previously visited neighborhood, are investigated in various dynamical regimes and are found to be in agreement with those of the finite-time Lyapunov exponents. The important advantages of the former ones are that they are easy to estimate and that comparable short time series are sufficient. Asymmetric distributions with exponential tails are observed for intermittency and crisis-induced intermittency, while for typical chaos, the distribution has a Gaussian shape. Further, the shape of the distribution distinguishes intermittent strange nonchaotic attractors from those appearing through fractalization and tori collision mechanisms. Furthermore, statistics performed on the peaks in the frequency distribution of recurrence times unveil scaling behavior in agreement with that obtained from the spectral distribution function defined as the number of peaks in the Fourier spectrum greater than a predefined value. The results of the present recurrence statistics are of relevance in classifying different dynamics and providing important insights into the dynamics of a system when only one realization of this system is available. The practical use of this approach for experimental data is shown on experimental electrochemical time series.

DOI: 10.1103/PhysRevE.85.026217 PACS number(s): 05.45.Pq, 05.45.Tp, 05.45.Ac

## I. INTRODUCTION

The concept of recurrences in dynamical systems has its origin from the work of Poincaré [1] who has shown that, under certain conditions, the orbit of a dynamical system returns arbitrarily into a neighborhood of each of its former points with probability one. A recurrence plot (RP) is a graphical representation of a matrix which receives the value one when the flow visits the vicinity of its previous points and is zero otherwise [2], events that are termed as recurrence and nonrecurrence, respectively. An example of a RP is given in Fig. 1, where the values one and zero are respectively plotted as gray and white dots.

Different recurrence quantification measures based on the statistical properties of the structures in the RPs have been introduced and applied to various fields ranging from earth sciences, via biology, to sociology [3,4]. In particular, the distributions of the lengths of vertical and diagonal lines formed by the recurrence points have been exploited in delineating different dynamical transitions that have been observed in various systems [3]. Recurrence-based techniques serve as remarkable tools in analyzing short, noisy, and observational time series [3]. The present work deals with statistics related to the vertical lines formed by the nonrecurrence points and therefore to the recurrence time.

The recurrence time (RT), defined as the time needed for a trajectory of a dynamical system to recur to a previously visited neighborhood, can be extracted from a RP. We have shown that the vertical nonrecurrence points, which are the white vertical lines in a RP, are a possible estimator of the RT [5]. Statistics developed on RTs have shown that the probability density function of RTs for well-developed chaos is exponential and some scaling laws relating the mean RT to the information dimension of chaotic attractors have been reported [6]. Furthermore, measures of complexity based on RTs were successfully applied to detect nonstationarity in time series and dynamical transitions from regular to chaotic behavior via strange nonchaotic dynamics [5–7].

Strange nonchaotic dynamics (SND) has been the subject of much interest, since it was reported by Grebogi *et al*. [8]. In the presence of a quasiperiodic forcing, SND usually appears as an intermediate stage between order and chaos in dynamical systems. Mechanisms for the birth of strange nonchaotic attractors (SNAs) in dynamical systems and tools for their characterization were reported in Ref. [9]. Among them, the distribution of finite-time Lyapunov exponents (FTLEs) [10,11] is widely used to characterize SNAs [12–18] and to distinguish the mechanisms of their birth. FTLEs measure the rate of separation of volume elements in the phase space and are computed over finite-time segments along a given trajectory [10–13]. A variant of these exponents, namely scale-dependent Lyapunov exponents, has been introduced and used to distinguish chaos from noise [19]. The distribution of FTLEs gives rise to typical structures for different dynamical behavior and has been applied to characterize the dynamics in a number of physical situations [10–18].

In the present work, we investigate the distribution of mean recurrence times (MRTs). This distribution is computed considering short segments of trajectory of a dynamical system. For each segment, a RP is computed and the related frequency distribution of RTs is extracted. The MRT is the mean of this frequency distribution and the distribution of MRTs is then the probability density of MRTs computed over all the considered short segments of trajectory. We show that the distribution of MRTs is capable of distinguishing various dynamics ranging from typical chaos, intermittency, and crisis-induced intermittency to different types of SNAs. In particular, the distribution of MRTs shows typical characteristic shapes

 

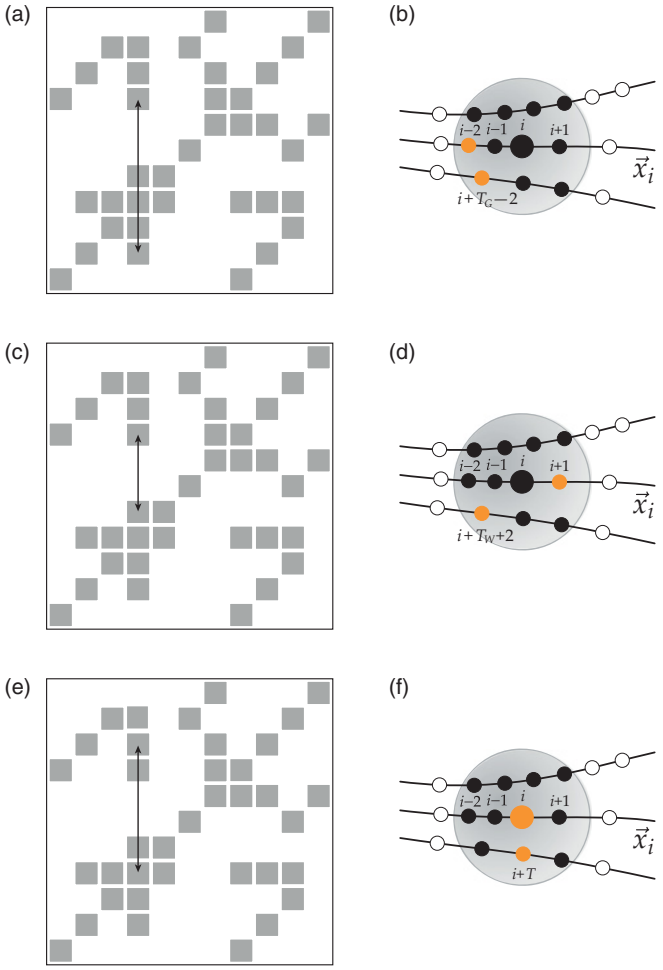


FIG. 1. (Color online) RP illustrating the estimators of RTs (black arrows), based on (a) distance between starting points [6] and (c) white vertical lines [5]. For vertically extended recurrence structures, both estimators differ and present upper and lower limits of the Poincaré RT, which would be actually the distance between the midpoints of the recurrence structures (e). (b), (d), (f) Recurrence points of a state $i$ illustrating the differences in the estimators for the RT $T$. (b) The estimator $\tilde{T}_G$ as defined by Gao [6] corresponds to the time distance between the first points falling into the neighborhood of state $i$ (here $i-2$ and $i+\tilde{T}_G-2$). (d) The estimator $\tilde{T}_W$ as defined by white vertical lines [5] corresponds to the time distance between the last and first points falling into the neighborhood of state $i$ (here $i+2$ and $i+\tilde{T}_W+2$). (f) The Poincaré RT $T$ for the illustrated case.

depending on the underlying dynamics. The distribution has a Gaussian shape for a typical chaos. For intermittency and crisis-induced intermittency, the distributions are asymmetric and possess an exponential tail. Among the different routes to SNAs, we have considered the Heagy-Hammel (HH) route [20], the fractalization of a torus (FT) [21], and the intermittency (IT) [18]. The distribution of MRTs is found to be asymmetric for SNAs created through these mechanisms; however, for intermittent SNAs an exponential tail or a slow decay in the tail is observed. We note that, in addition to the good agreement of the distribution of MRTs with that of FTLEs, MRTs have the advantage of their easy estimation also for real-world data, which are usually short and noisy.

Furthermore, in this work, in analogy with the spectral distribution function, we quantify the peaks in the frequency distribution of RTs extracted from RPs. We have found that quasiperiodic dynamics and SND show a logarithmic and a power law behavior, respectively, in agreement with that of their spectral distribution function [22]. In the following, we demonstrate our results in the logistic map in the regimes of typical chaos, type-I IT and crisis-induced IT and transitions to SNAs (for the above three routes and also in a Duffing oscillator). To corroborate the practical application of the proposed recurrence statistics to real-world data, we illustrate it on experimental data from an electrochemical cell.

The paper is organized as follows. After explaining how RTs and MRTs can be extracted from RPs in Sec. II, the characteristic distributions of MRTs corresponding to different dynamics are presented in Sec. III. We describe in Sec. IV the statistics on the peaks in the frequency distribution of RTs. These recurrence based statistics are applied to electrochemical experimental data in Sec. V. This is followed by a summary in Sec. VI.

## II. RECURRENCE TIME AND MEAN RECURRENCE TIME EXTRACTED FROM RPS

### A. Recurrence time

Given a trajectory, $\{\vec{\mathbf{x}}_i\}_{i=1}^{L}$, of a dynamical system where $\vec{\mathbf{x}}_i \in \mathbb{R}^n$, the RP efficiently visualizes its recurrences and can be formally expressed by the matrix

$$\mathbf{R}_{i,j} = \Theta(\delta - \|\vec{\mathbf{x}}_i - \vec{\mathbf{x}}_j\|), \quad i,j = 1,\ldots,L, \tag{1}$$

where $\delta$ is a predefined threshold, $\Theta(\cdot)$ is the Heaviside function, and $\|\cdot\|$ denotes a norm (here the maximum norm). In the coordinate $(i,j)$ of the RP, we can choose black to plot a point if $R_{i,j}=1$ and white otherwise. As already mentioned, a RT is the time needed for a trajectory of a dynamical system to return into the neighborhood of a previously visited point in the phase space. Poincaré RTs can be estimated directly from a RP, since the distance between recurrence points in a column of the RP corresponds to the duration until a state recurs. However, due to consecutive points on a phase space trajectory falling into the neighborhood of the considered state (resulting in vertically extended structures in the RP; cf. Fig. 1), some of these RTs correspond to the tangential motion but not to the dynamics of the system [3]. Therefore, Gao [6] has suggested to remove such consecutive recurrence points in a column of the RP when measuring RTs. This estimator of RTs coincides with the vertical distance between the starting point of a recurrence structure with the starting point of the next recurrence structure, as shown in Figs. 1(a) and 1(b). Such RTs have been called RTs of second type [6].

We have recently proposed another estimator for the RT which is based on the length of the white vertical lines in a RP [5]. This estimator corresponds to the vertical distance between the end point of a recurrence structure and the starting point of the next one, as illustrated in Figs. 1(c) and 1(d). Note that both Gao's and the white vertical lines approaches for estimating RTs differ from the Poincaré RTs if the recurrence structures have some vertical extensions (i.e., lines of thickness larger than 1, for example, for highly sampled continuous

systems [3]). For such cases the Poincaré RT would be better estimated by using the (vertical) midpoints of the recurrence structures [Figs. 1(e) and 1(f)]. The RT as defined by Gao is, therefore, an upper limit and the RT based on white vertical lines is a lower limit of the Poincaré RT.

All the three previously defined estimators allow a reliable computation of the RT from RPs and they give similar results as long as the recurrence structures in the RP are mainly not vertically extended. In the present work, we have chosen the definition based on the white vertical lines because it is straightforward. Moreover, for the systems and their corresponding parameter values considered in this work we usually do not encounter vertical extensions in the RPs constraining us to use the estimator described in Figs. 1(e) and 1(f).

### B. Mean recurrence time

For a given trajectory of length $L$, the MRT $M_L$ is obtained by computing the mean of the frequency distribution $p(k)$ of white vertical lines of lengths $k$ as

$$M_L = \frac{\sum_{k=1}^{L} kp(k)}{\sum_{k=1}^{L} p(k)}. \tag{2}$$

The distribution of MRTs is obtained by dividing a given trajectory into short segments of length $N$ and computing the MRT corresponding to each segment. The probability density $P(M,N)$ of MRTs computed over all the short segments is defined as the probability that $M$ takes a value between $M$ and $M + dM$ and it reveals typical structures depending on the nature of the underlying dynamics, as we demonstrate in the next section. To investigate how the distribution of MRTs changes with changes of parameters $\delta$ and $N$, we consider the variance of MRTs.

The recurrence statistics proposed in this work depend on the threshold $\delta$ used to compute the recurrence matrix of Eq. (1). For very small $\delta$, the RP has less or even no recurrence points leading to a lack of enough information embedded in the recurrence structures of the underlying system. Increasing $\delta$ increases the number of recurrence points and other diagonal or vertical recurrence structures in the RP. A further increase of $\delta$ still increases the number of recurrence points and can lead to thicker diagonal lines or a merging of some diagonal lines. As a consequence, some peaks in the frequency distribution $p(k)$ are no longer existing or are reduced and the distribution becomes simpler. In such situations, it can give rise to a reduction of the MRT and a reduction of its variance. Further increase to very large $\delta$ produces RPs in which almost every point is a neighbor of every other point, which, in turn, results in a loss of meaningful recurrence structures.

On the other hand, very small or high $\delta$ values do not always lead to difficulties. It has been shown, for example, that in the presence of noise large thresholds are preferable because such thresholds preserve structures in the RP [3]. The choice of $\delta$ depends not only on the dynamics but also on the considered system under study. A lot of effort have been devoted to provide approaches for reliably choosing $\delta$. Several methods have been reported in the literature ([3,4,23,24], to cite a few) and they were successfully applied for different systems and dynamics also from real life. It would be pretentious to say that the choice of $\delta$ has been investigated for all the existing systems; however, for a broad band of systems and dynamics, the available approaches in the literature make it possible to make a reliable choice. Throughout this work, we have fixed $\delta$ as a certain percentage of the standard deviation $\sigma$ of the data and whose value is specified at appropriate places in the paper.

The length $N$ of the segments trajectory also plays a role in the present recurrence statistics. To apply the statistics it is necessary that the chosen $N$ contains sufficiently enough dynamics for a reliable computation of the RP. We expect that for very short $N$, just small pieces of the underlying attractor are considered. The probability that each of the short considered segments displays a different dynamics (or each segment has information that no other has) is high. The similarity ($S$) in the amount of information or dynamics reflected by the short trajectory segments is then rather low. The frequency distribution $p(k)$ (therefore, MRT) will then change drastically over the segments. The variance of MRTs can then be large. Increasing $N$ increases the considered portions of the underlying attractor. It is becoming possible to observe common pieces of information or dynamics reflected in the trajectory segments. This increase of $S$ is also reflected in $p(k)$ (therefore in MRT) and it can lead to a decay of the variance. Further increase of $N$ increases $S$. For $N$ large enough such that almost all the underlying (or the entire) attractor is covered by each segment, $S$ in all the segments [hence in the respective $p(k)$ and MRT] is very high and one may then expect further decay of the variance.

In the following, in order to compare and to correlate the typical structures of the distribution of MRTs corresponding to a particular dynamics, the distribution of FTLEs is also estimated. Contrary to the asymptotic Lyapunov exponent computed over long intervals of time, FTLEs depend on the initial conditions and their distributions depend on the length of the time series over which the FTLEs are computed [25].

## III. DISTRIBUTIONS OF MRTS IN CHAOTIC, INTERMITTENCY AND CRISIS DYNAMICS AND THROUGH TRANSITIONS TO SNAS

### A. Typical chaos

To clarify the notion of typical chaos, we use the properties of correlation functions which play an important role in characterizing chaotic systems. For systems exhibiting typical chaotic dynamics the corresponding correlation functions decay exponentially, whereas for systems exhibiting well developed chaos the decay of correlations is slower than exponential. It has been shown that for typical chaos the central limit theorem [26] holds for a number of averaged quantities including FTLEs [13,14]. It implies that the distribution of FTLEs is Gaussian. Now we show that the distribution of MRTs acquires a Gaussian distribution as that of the FTLEs in a typical chaotic regime of the logistic map,

$$x_{n+1} = \alpha x_n(1 - x_n), \tag{3}$$

for the value $\alpha = 3.7$ at which one encounters bands of unstable periodic orbits which are absent in the fully developed chaos which occurs at $\alpha = 4$. Distributions of MRTs and

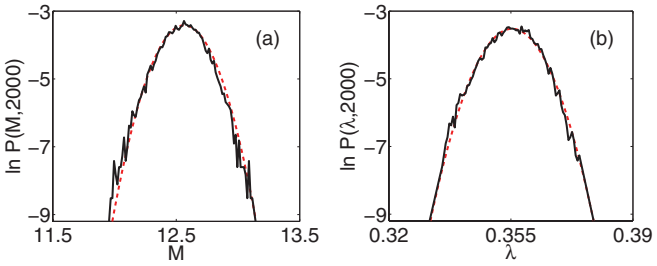


FIG. 2. (Color online) Probability density of (a) MRTs and (b) FTLEs, computed from the logistic map Eq. (3), with $\alpha = 3.7$ giving rise to a typical chaos and the threshold $\delta = 0.1\sigma$, where $\sigma$ is the standard deviation of the data. For each case a Gaussian (dashed red line) is fitted on the distribution.

FTLEs are estimated from a trajectory consisting of $10^4$ segments where each segment is of length $N = 2000$ samples. The probability densities $P(M,N)$ of MRTs and $P(\lambda,N)$ of FTLEs are shown in Figs. 2(a) and 2(b), respectively. The distribution of MRTs displays a Gaussian shape as reported in the case of FTLEs for a typical chaos [16]. The Gaussian fit to the distributions using the function $f(x) = ae^{-\frac{(x-b)^2}{2c^2}}$ (for the values of $a = 0.032$, $b = 12.56$, and $c = 0.17$ for MRTs and $a = 0.029$, $b = 0.355$, and $c = 0.007$ for FTLEs) are also shown in Figs. 2(a) and 2(b). The parameters $a$ and $b$ are the height of the curve's peak and the position of the center of the peak, respectively, while $c$ controls the width of the bell.

The dependence of the variance of FTLEs on $N$, examined for various dynamics in Ref. [16], has revealed a power law behavior and an exponent of decay equal to 1.12 was reported for a typical chaos. We have analyzed the variance of MRTs for a broad range of $N$ and $\delta$ values, which is shown in Fig. 3. The value of $N$ was increased up to 9000 samples, while $\delta$ was increased up to $0.2\sigma$. This value of $\delta$ is sufficient in accordance with the rules for choosing $\delta$, which recommend that $\delta$ should be chosen as a few percent of the maximum phase space diameter and it should not exceed 10% of the mean or the maximum phase space diameter [23,24]. For each value of $N$ and $\delta$, the variance was computed over 2000 segments of length $N$ and it decays as shown in Fig. 3. To exemplify this decay of the variance, $N$ is varied as $\delta$ is fixed at $0.03\sigma$, $0.06\sigma$, and $0.1\sigma$ in Fig. 4(a). Similarly, $\delta$ is varied as $N$ is fixed at $N = 2000$, $N = 4000$, and $N = 8000$ in Fig. 4(b). Note that the respective fixed values of $N$ and $\delta$ were randomly chosen and are considered just for illustrative purposes.

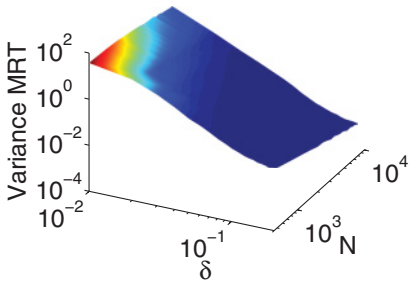


FIG. 3. (Color online) Variance of MRTs in dependence on $N$ and $\delta$ for a typical chaos in the logistic map Eq. (3), with $\alpha = 3.7$. All the axes are in log scale.

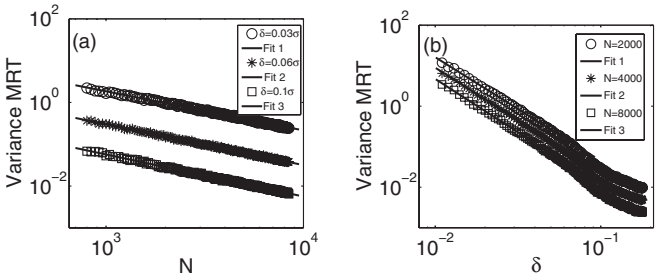


FIG. 4. Illustration of the decay of the variance of MRTs observed in Fig. 3 for (a) fixed thresholds $\delta = 0.03\sigma$, $\delta = 0.06\sigma$, and $\delta = 0.1\sigma$ as $N$ varies and (b) fixed $N = 2000$, $N = 4000$, and $N = 8000$ as $\delta$ varies. Both axes are in log scale.

The variance scales as $N^{-\gamma_N}$, with $\gamma_N = 0.9350 \pm 0.0032$, $\gamma_N = 0.9766 \pm 0.0029$ and $\gamma_N = 1.0053 \pm 0.0034$ for the respectively fixed $\delta$ [Fig. 4(a)]. For the fixed $N$, the variance evolves as $\delta^{-\gamma_\delta}$ just for low values of $\delta$ [in Fig. 4(b)], with $\gamma_\delta = 2.5599 \pm 0.0117$, $\gamma_\delta = 2.5914 \pm 0.0127$, and $\gamma_\delta = 2.6352 \pm 0.0149$, respectively. For the higher values of $\delta$ [in Fig. 4(b)] the variance keeps decaying but not as a power law. The power law decay of the variance of MRTs as a function of $N$ suggests that the distribution of MRTs narrows as $N$ increases. Further, this power law decay is in agreement with that of FTLEs reported in Ref. [16]. In the next section, distributions of FTLEs and MRTs are investigated in other typical regimes of complex systems: IT and crisis-induced intermittency.

### B. Intermittency and crisis-induced intermittency

In chaotic systems, three different types of IT have been reported and are related to three different inverse bifurcations [27]. We consider here type-I IT, which appears generally close to an inverse saddle-node bifurcation. We consider it in the logistic map, near the period-3 window or near the tangent bifurcation. The dynamics exhibits trajectories which stay close to the period-3 orbit (and which form the laminar phase) and some turbulent chaotic bursts. Its distribution of FTLEs was reported to be asymmetric, exhibiting a sort of departure from a normal density and an exponential tail [10,16]. The tail part could be regarded as a contribution of trajectories which after staying in the laminar region for some time bounce out from this region, make an excursion in the irregular region, and come back again into the laminar one. However, the distributions of FTLEs for both the laminar phase and the irregular chaotic bursts when considered separately have, respectively, a normal density as seen, for example, for the chaotic dynamics in Fig. 2.

We also consider crisis-induced IT. It occurs where an unstable period-$n$ orbit collides with a chaotic attractor consisting of $n$ pieces and when a chaotic attractor collides with a chaotic saddle to form a much larger chaotic attractor [9]. The remarkable features which happen after the collision are the sudden widening of the chaotic attractor and the reduction of the number of its pieces. Because of the widening of the attractor, some trajectories bounce out from the region of the phase space where they were confined before the crisis and make a long excursion into the new region, which was made

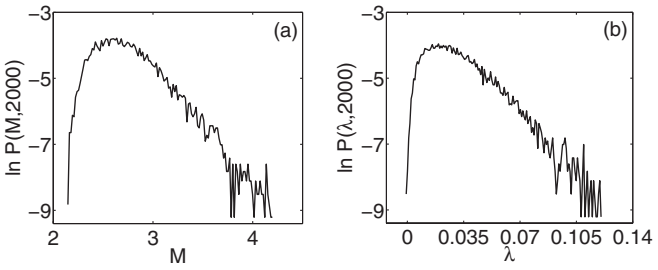


FIG. 5. Probability density of (a) MRTs and (b) FTLEs, computed using the threshold $\delta = 0.1\sigma$ and data from the logistic map Eq. (3), with $\alpha = 1 + \sqrt{8} - 10^{-6}$ for which type-I IT is observed.

available by the widening of the attractor, and come back into their starting region. These trajectories contribute to the tail part of the distribution of FTLEs for crisis dynamics, which was reported to exhibit a departure from a normal density and a tail [16].

We have investigated the distributions of MRTs and compared them to those of FTLEs for the above dynamics. We exemplify these distributions in the logistic map Eq. (3) for $\alpha = 1 + \sqrt{8} - 10^{-6}$ close to which the dynamics is of type-I IT and for $\alpha = 3.744\,710\,4$, at which an interior crisis occurs. The distributions were computed using $10^4$ segments with $N = 2000$ samples each. The distributions of MRTs and FTLEs are shown in Figs. 5 and 6 for type-I IT and crisis, respectively. The distributions of MRTs are asymmetric with an exponential tail as the distributions of FTLEs. For type-I IT, we have also analyzed values of $\alpha$ which are not very close to the tangent bifurcation point and the corresponding distributions are in agreement with those shown in Fig. 5.

The dependence of the variance of FTLEs on $N$ for the above dynamics was reported to display a power law behavior; however, for type-I IT a crossover was observed since the exponents in different ranges of $N$ go from an exponential limit to a Gaussian limit at large $N$ [16]. We have investigated the dependence of the variance of MRTs on $N$ and $\delta$ for the above dynamics. The first information we get from this investigation is that for both dynamics the variance decays for a wide range of $\delta$ and $N$ values, similar as in Fig. 3. We note further that this decay is a power law as $N$ is increased while $\delta$ is kept fixed. Finally, we note that the exponential tail in the distribution of MRTs gradually disappears as $N$ increases and for large $N$ the distribution tends to a Gaussian.

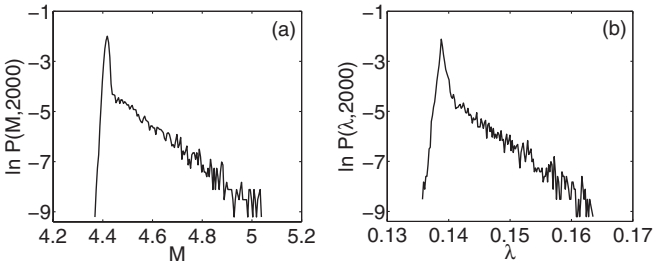


FIG. 6. Probability density of (a) MRTs and (b) FTLEs, computed using the threshold $\delta = 0.1\sigma$ and data from the logistic map Eq. (3), with $\alpha = 3.744\,710\,4$ for which an interior crisis occurs.

From the results shown up to this point, we can conclude that the shape of the distributions of MRTs and FTLEs can be used to distinguish typical chaos from type-I IT and crisis dynamics. We have performed Kolmogorov-Smirnov (KS) tests to infer how significant the distributions differ through these dynamics. Our null hypothesis (HO) is that the distributions do not differ significantly. Comparing the distribution of MRTs (respectively, distribution of FTLEs) for typical chaos to that of IT [Figs. 2(a) and 5(a); Figs. 2(b) and 5(b)], the KS test at a 1% level of significance rejects the HO with the $p$ values $p = 0.002$ and $p = 5.69 \times 10^{-6}$, respectively. Comparing the distributions of typical chaos to those of crisis-induced IT [Figs. 2(a) and 6(a); Figs. 2(b) and 6(b)], the KS test rejects the HO with the $p$ values $p = 6.12 \times 10^{-5}$ and $p = 1.10 \times 10^{-7}$. The KS tests confirm that the distributions differ significantly through the considered dynamics. Although the distributions for type-I IT and crisis dynamics show similar global characteristics as shown in Figs. 5 and 6, the $p$ values ($p = 9.22 \times 10^{-4}$ and $p = 0.002$) obtained when comparing their respective distributions [Figs. 5(a) and 6(a); Figs. 5(b) and 6(b)] suggest that these distributions differ as well. Further statistics have to be performed to distinguish them and this is an interesting topic for future work.

### C. Transitions to strange nonchaotic attractors

We focus now on the distributions of MRTs for SND. This dynamics lies in between quasiperiodic motion and chaos. Like in regular dynamics, the nonchaoticity is related to the absence of sensitive dependence on initial conditions. The strangeness refers to the fractal structure of the attractors similar to that of chaotic attractors. SND has been reported in many systems ranging from maps and continuous systems to experimental devices [9]. Different mechanisms through which SNAs can arise in a forced system have been reported. We have focused on the following ones: (i) HH route, in which a period-doubled torus collides with its unstable parent and a SNA is then created [20]; (ii) FT, in which a torus becomes more and more wrinkled until it breaks to form a SNA [21]; (iii) IT route in which a SNA is created through a saddle-node bifurcation [18]. SND has been reported in quasiperiodically forced maps and since two-dimensional invertible maps could be regarded as Poincaré sections of three-dimensional flows, SND could also be observed in flows. In the following, we exemplify the distributions of MRTs through the above transitions to SNAs in a map and a continuous system.

#### 1. Transitions to SNAs in a map

We consider the following quasiperiodically forced logistic map:

$$x_{n+1} = \alpha[1 + \varepsilon'(4/\alpha - 1)\cos(2\pi\theta_n)]x_n(1 - x_n),$$
$$\theta_{n+1} = \theta_n + \omega \pmod 1, \tag{4}$$

where the quasiperiodic forcing is applied by making a rotation of the phase variable $\theta$ with the irrational frequency $\omega = (\sqrt{5} - 1)/2$. The term $\varepsilon'(4/\alpha - 1)$ represents the forcing amplitude. The parameters $\alpha$ and $\varepsilon'$ take different values according to the mechanism through which the SNA is created and are specified in the figure caption of Fig. 7. The

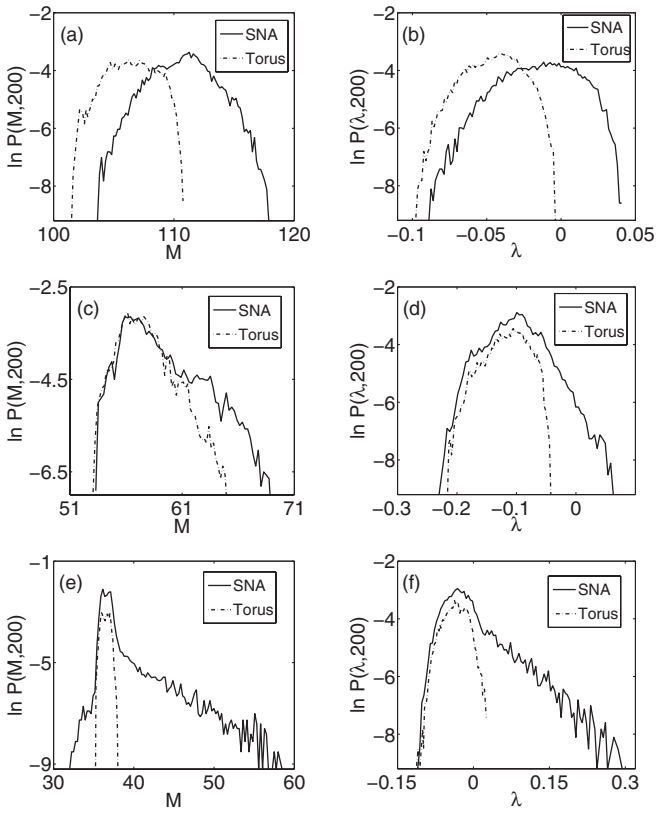


FIG. 7. Distribution of MRTs (a), (c), (e) and FTLEs (b), (d), (f) through transitions to SNAs in the logistic map Eq. (4). (a), (b) FT route, $\varepsilon' = 1$, $\alpha = 2.63$ for torus, and $\alpha = 2.66$ for SNA; (c), (d) HH route, $\varepsilon' = 0.3$, $\alpha = 3.4874$ for torus, and $\alpha = 3.488$ for SNA; (e), (f) IT route, $\varepsilon' = 1$, $\alpha = 3.405\,81$ for torus, and $\alpha = 3.405\,805\,6$ for SNA.

distributions of FTLEs for the above system through transitions to SNAs have been reported in Ref. [17]. Distributions of FTLEs through transitions to SNAs in other dynamical systems have also been investigated; however, in the works found in the literature no clear distinction criteria on the shape of the distribution for FT and HH routes are given. For these mechanisms the distributions are reported to tend to a Gaussian even though they do not fulfill all criteria of a Gaussian. More generally, it has been observed that the distributions are asymmetric [16–18,28,29]. However, for intermittent SNAs clear criteria that the distribution of FTLEs fulfills are reported: The distribution displays a departure from a Gaussian part followed by a (stretched) exponential tail [16–18,28,29]. These criteria allow one to distinguish intermittent SNAs from fractalized and HH SNAs.

For each route to SNAs, we have investigated the distributions of MRTs for a torus prior to the transition to SNAs and for a SNA just beyond the transition. The transition from a torus to a SNA is subtle because both attractors have common properties and a global stable dynamics. Usually the torus very close to the transition to SNAs has visually almost the same appearance as the SNA. One major difference between both attractors is the fractal structure of the SNA, which could be shown using some subtle techniques, among them the phase sensitivity function [9]. One may then not expect a large difference between distributions of MRTs on torus and SNA in the same process except for the IT mechanism, since intermittent SNAs are morphologically quite distinct from those formed through the FT and HH routes. On fractalized SNAs, points on the attractor stay close to the parent torus (see Fig. 1 of Ref. [21]). On HH SNAs the points are distributed within the entire region enclosed by the wrinkled bounding tori (see Fig. 1 of Ref. [20]), while on the intermittent SNAs, most points remain near the parent torus with sporadic large deviations [17,18]. For each mechanism the distributions of MRTs, computed using both coordinates $x$ and $\theta$, $10^4$ segments with $N = 200$ samples each and the threshold $\delta = 0.1\sigma$ ($\sigma$ being the standard deviation of the $x$ coordinate) are shown along with the distributions of FTLEs in Fig. 7 for a torus prior to the transition to SNAs and for a SNA just beyond the transition. The asymmetric distributions of MRTs in Figs. 7(a) and 7(c), and those of FTLEs in Figs. 7(b) and 7(d) correspond to FT and HH routes, respectively. In Figs. 7(e) and 7(f) both distributions are also asymmetric; however, a clear deviation from a normal density and a pronounced tail are observed. These are typical characteristics of IT.

We have performed KS tests to infer how significantly the distributions for intermittent SNAs differ from those of fractalized and HH-SNAs. Our HO is that the distributions do not differ. Comparing the distribution of MRTs (respectively distribution of FTLEs) of fractalized and intermittent SNAs [Figs. 7(a) and 7(e); Figs. 7(b) and 7(f)], the KS test at a 10% level of significance rejects this HO with the $p$ values $p = 6.09 \times 10^{-9}$ and $p = 0.005$, respectively. Comparing the distributions of HH and intermittent SNAs [Figs. 7(c) and 7(e); Figs. 7(d) and 7(f)], the KS test rejects the HO with the $p$ values $p = 2.68 \times 10^{-13}$ and $p = 0.067$, respectively. The KS tests confirm that the distributions of MRTs and FTLEs of intermittent SNAs differ significantly from those of fractalized and HH SNAs. The shape of the distributions can then be used to distinguish among them.

### 2. *Transitions to SNAs in a continuous system*

We consider now a damped, two-frequency driven Duffing oscillator represented as

$$\begin{aligned} \dot{x} &= y, \\ \dot{y} &= -hy + [1 + A(R\cos(\phi) + \cos(\theta))]x - x^3, \\ \dot{\phi} &= 1, \\ \dot{\theta} &= \Omega, \end{aligned} \qquad (5)$$

where the parameters $A = 0.3$ and $\Omega = (\sqrt{5}+1)/2$ are fixed, while $h$ and $R$ are varied through the transitions to SNAs. A simple experimental realization of this system, the magnetoelastic ribbon, has been extensively studied [30], and it is the first system where SNAs were observed experimentally [31]. Different transitions to SNAs have been reported in this system for different values of $h$ and $R$ [28], which we have adapted in the present work to investigate the shapes of the distributions of MRTs through these transitions: $R = 0.47$ for FT, 0.3 for HH, and 0.35 for IT; $h = 0.0729$ and 0.072 in FT, 0.184 and 0.181 in HH, and 0.190 885 64 and 0.190 833 in IT for torus and SNA, respectively. The system is integrated using a fourth-order Runge-Kutta algorithm with the integration

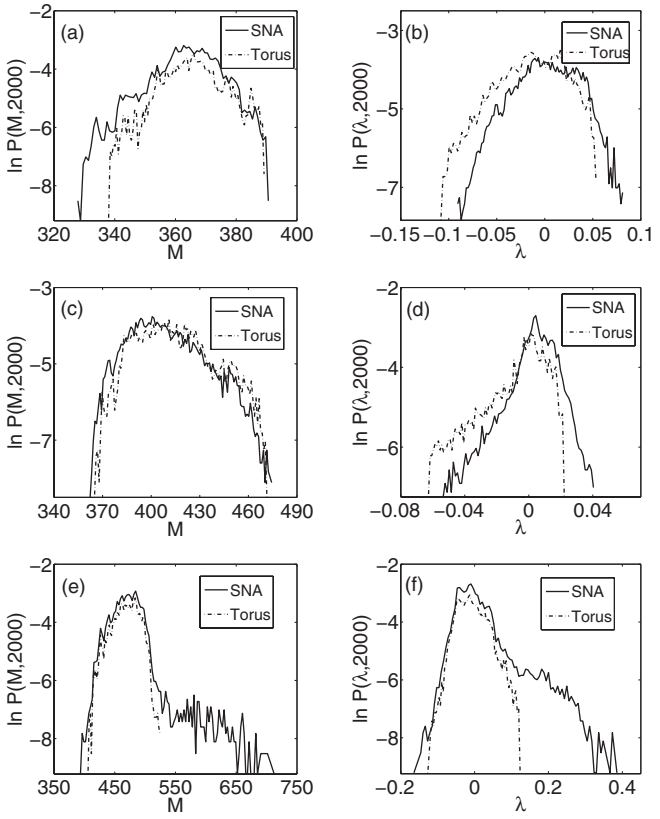


FIG. 8. Distributions of MRTs (a), (c), (e) and FTLEs (b), (d), (f) through transitions to SNAs in the system Eq. (5). (a), (b) FT route; (c), (d) HH route; (e), (f) IT route.

step $H = 2\pi/100\Omega$. Both coordinates $x$ and $y$ are used and no embedding is performed. After neglecting sufficient transient, the distributions of MRTs are computed using $10^4$ segments with $N = 2000$ integration steps and the threshold $\delta = 0.1\sigma$ ($\sigma$ being the average of the standard deviation of $x$ and $y$ coordinates, respectively). The distributions of MRTs are shown along with those of FTLEs in Fig. 8 for all the three routes. The distributions are asymmetric and those corresponding to the IT transition [Figs. 8(e) and 8(f)] exhibit a deviation from a normal density and a pronounced tail, similar as the ones observed in other distributions shown in the previous subsections [Figs. 5, 6, 7(e), and 7(f)].

Using the previously stated HO, we have again performed KS tests to compare the distibution of MRTs (respectively, distribution of FTLEs) of fractalized and intermittent SNAs [Figs. 8(a) and 8(e); Figs. 8(b) and 8(f)] on the one hand and the distributions of HH and intermittent SNAs [Figs. 8(c) and 8(e); Figs. 8(d) and 8(f)] on the other hand. The KS tests at a 10% level of significance reject the HO with the $p$ values $p = 5.10 \times 10^{-11}$ (respectively, $p = 1.91 \times 10^{-4}$) on the one hand and $p = 9.93 \times 10^{-12}$ (respectively, $p = 0.013$) on the other hand. It indicates that the distributions of MRTs and FTLEs of intermittent SNAs differ significantly from those of the other SNAs. These distributions can hence distinguish intermittent SNAs from fractalized and HH SNAs in a continuous system.

From the results of Figs. 7 and 8, we conclude at this point that the distributions of MRTs can differentiate intermittent SNAs from the other SNAs in both maps and continuous systems. However, we note that methods which are usually straightforward for maps are not always appropriate for continuous systems. For example, the discrete time sampling for maps usually ensures enough dynamics even for short segments of data. With continuous systems, the sampling rate should be chosen suitably and allow us to acquire sufficiently enough dynamics in the considered short segment of trajectory, leading to a reliable computation of the RP. It has been shown that even for very simple signals, such as sinusoids, the sampling time can introduce an intrinsic phase error to which RPs are sensitive [32].

We have studied the dependence of the variance of MRTs on $N$ and $\delta$ for the SNAs investigated in the logistic map Eq. (4) and the continuous system Eq. (5). For each value of $N$ and $\delta$, the variance was computed over 1000 segments of length $N$. For both systems and for the three SNAs, we note that the variance of MRTs globally decays similarly as in Fig. 3. Another useful information is that the variance decays as a power law as $N$ is increased while $\delta$ is kept fixed. Finally, we note that as $N$ is increased to large values, the tail in the distribution of MRTs for intermittent SNAs vanishes progressively, while the distributions of MRTs for fractalized and HH SNAs narrow. This suggests that for very large $N$, the tail could totally disappear, leading that the distribution could tend to a Gaussian and therefore the distinction of intermittent SNAs from other SNAs will be difficult. However, for a wide range values of $N$ including small ones, this distinction is clearly possible. This is advantageous for observational data where usually short data are available only.

## IV. SCALING BEHAVIOR FROM FREQUENCY DISTRIBUTIONS OF RECURRENCE TIMES

In this section, in analogy with the spectral distribution function (SDF), we quantify the peaks in the frequency distribution [$p(k)$ in Eq. (2)] of RTs of lengths $k$ extracted from RPs of quasiperiodic attractors and SNAs. In particular, we count the number of peaks in $p(k)$ which are greater than a predefined value. We observe that this number scales as a logarithmic and power law behavior for two-frequency quasiperiodic motion and SNAs, respectively. These scaling behaviors are in agreement with those reported for the SDF defined as the number of peaks in the Fourier spectrum greater than a predefined value [22].

For our illustration, we use the following system [33]:

$$\frac{1}{p}\ddot{x} + \dot{x} - \cos(x) = K + V[\cos(\omega_1 t) + \cos(\omega_2 t)], \qquad (6)$$

where $\omega_1 = (\sqrt{5}-1)/2$, $\omega_2 = 1$, and $p = 3$. $K$ and $V$ are the bifurcation parameters. We have integrated the above system using a fourth-order Runge-Kutta method with 32 time steps per period of $\cos(\omega_2 t)$ and recorded 10 000 data points. We have considered (i) a two-frequency quasiperiodic motion occurring for $K = 1.34$ and $V = 0.55$ and (ii) a SNA for parameter values $K = 1.33$ and $V = 0.55$. Their respective RPs were computed for $\delta = 0.1\sigma$ ($\sigma$ being the average of the standard deviation of $x$ and $\dot{x}$ coordinates, respectively) and the peaks in the distribution $p(k)$ from these RPs were quantified. Varying a threshold $S$ corresponding to the height of the peaks in $p(k)$ from the minimum to the maximum value of $p(k)$,

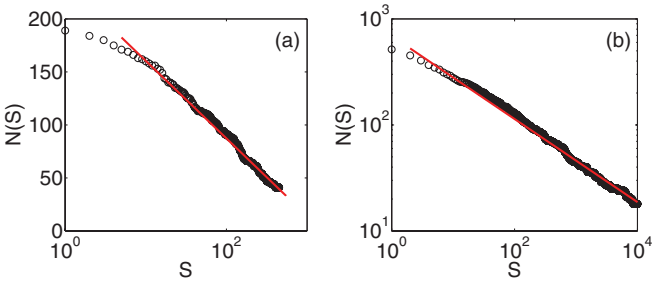


FIG. 9. (Color online) Number of peaks $N(S)$ in the frequency distribution of RTs which are greater than a predefined threshold $S$ (circles). (a) Two-frequency quasiperiodic motion, and (b) SND. The solid line in (a) corresponds to the scaling relation $N(S) \sim \ln(1/S)$ and in (b) to the scaling relation $N(S) \sim S^{-\gamma}$, with $\gamma = 0.39 \pm 0.0003$. The plots are shown in semilog and log-log axes for (a) and (b), respectively.

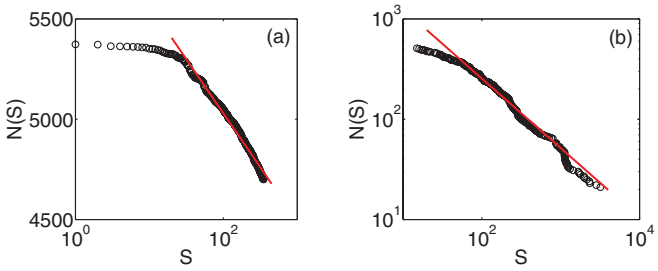


FIG. 11. (Color online) From experimental data: number of peaks $N(S)$ in the frequency distribution of RTs which are greater than a predefined threshold $S$ (circles). (a) Quasiperiodic motion; (b) SNA. The solid line in (a) corresponds to the scaling relation $N(S) \sim \ln(1/S)$ and in (b) to the scaling relation $N(S) \sim S^{-\gamma}$, with $\gamma = 0.69 \pm 0.007$. The plots are shown in semilog and log-log axes for (a) and (b), respectively.

we count the number of peaks $N(S)$ which are greater than $S$. We note that $N(S)$ differs for both the considered attractors as shown in Fig. 9. For the quasiperiodic motion, $N(S)$ evolves as a logarithmic function [Fig. 9(a)], while for the SNA a power law behavior with a scaling exponent $\gamma = 0.39 \pm 0.0003$ is observed [Fig. 9(b)].

We have performed the same analysis with quasiperiodic attractors and SNAs from other dynamical systems reported in Refs. [22,34,35] and found similar scaling behavior as those shown in Fig. 9. We have investigated the dependence of $N(S)$ on the threshold $\delta$ and the length $L$ of the trajectory. For the quasiperiodic dynamics (respectively for the SNA), the evolution of $N(S)$ as a logarithmic function (respectively as a power law) persists even for a large range of $\delta$ and $L$. In the following, we demonstrate that the scaling relations from the peaks in the frequency distribution of RTs and the distribution of MRTs are capable of distinguishing dynamics in experimental time series from an electrochemical cell.

## V. APPLICATION TO EXPERIMENTAL ELECTROCHEMICAL DATA

Recently, Ruiz *et al.* have experimentally observed SNAs in a driven excitable system [36]. The experimental setup is an electrochemical cell configured to study the potentiostatic electrodissolution of iron in a mixture of copper sulfate and sulfuric acid. The anode was pure iron. The cathode was a 5-mm-diameter copper rod. The electrolyte solution was a mixture of 1.0M sulfuric acid and 0.4M copper sulfate. A volume of about 500 ml was maintained in the cell. The anodic potential ($V$) was used as the bifurcation parameter onto which quasiperiodic perturbations were superimposed. The system observable is the anodic current, which is the current between the anode and the cathode. Oscillations of this current were recorded using a 12-bit data acquisition card at a sampling rate of 250 Hz.

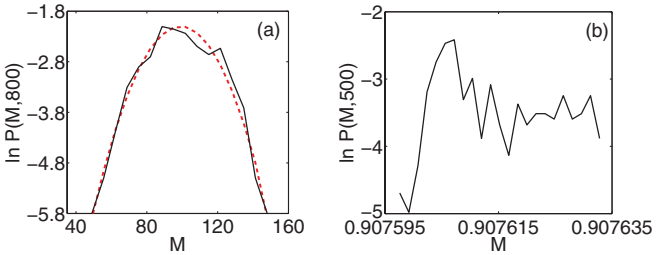


FIG. 10. (Color online) Probability density of MRTs computed from experimental electrochemical data (black solid line): (a) quasiperiodic motion; (b) SNA. The dashed red line is a Gaussian fit.

We have analyzed the data corresponding to a quasiperiodic motion and a SNA recorded in this experiment. For both the torus and SNA, distributions of MRTs are computed using the threshold $\delta = 0.2\sigma$ and segments of trajectory with $N = 800$ and $N = 500$ data points, respectively, which are shown in Fig. 10. A Gaussian (dashed red line) is fitted on the distribution of MRTs for the torus [Fig. 10(a)], while for the SNA, the distribution exhibits a sort of departure from a normal density followed by a tail which are due to two distinct time scales related to the excitable dynamics exhibited by the electrochemical cell [Fig. 10(b)]. This distribution is in agreement with that of SNAs created through IT and investigated in Sec. III. The number of peaks $N(S)$ in the frequency distribution of RTs which are greater than a predefined threshold $S$ is also calculated and is shown in Fig. 11. A logarithmic behavior is fitted on $N(S)$ for the quasiperiodic motion [Fig. 11(a)], whereas $N(S)$ for the SNA has a power law behavior with an exponent of $0.69 \pm 0.007$ [Fig. 11(b)].

From the results obtained in this section, one can see that, given an experimental set of data or data from the real world, the shape of the distribution of MRTs and the scaling behavior of the peaks in the frequency distribution of RTs can be used to identify the underlying dynamics and to differentiate between dynamics when it is needed. Further, these results confirm that the proposed recurrence statistics can be successfully applied on noisy and short time series.

## VI. SUMMARY

We have investigated properties of the distribution of MRTs and scaling behavior of the peaks in the frequency distribution of RTs in different dynamical regimes such as IT, crisis, quasiperiodic, and SND. We have compared our

results with the distribution of FTLEs and the scaling behavior of the spectral distribution function which have been widely exploited in the literature in distinguishing different dynamical behaviors. In particular, we have shown that the distribution of MRTs shows a Gaussian for typical chaos, while for type-I IT and crisis-induced IT, the distribution exhibits a departure from a normal density followed by an exponential or elongated tail as reported for the distribution of FTLEs in the corresponding regimes. We note that, in addition to a good agreement of the distribution of MRTs with that of FTLEs, MRTs have the advantage of their easy estimation also in situations where the equations of motion of the underlying system are not readily available.

Further, we have also investigated the distribution of MRTs for different types of SNAs. The distribution is asymmetric for SNAs created through FT, HH, and IT routes. However, for the IT case a deviation from a normal density followed by a pronounced tail can be observed and it allows one to distinguish intermittent SNAs from the other ones. The scaling laws extracted from the peaks in the frequency distribution of RTs of tori and SNAs show a logarithmic and a power law behavior, respectively, as observed from their corresponding spectral distribution function. Furthermore, we have also shown that these scaling laws and the distribution of MRTs are capable of characterizing the dynamics in experimental data from an electrochemical cell.

The results of the proposed recurrence statistics are of relevance in classifying different dynamics and providing useful information on the dynamics of the system when only one realization of the system is available and one wishes to infer in which dynamical regime the system is. They are also of practical use in presence of real-world data.

## ACKNOWLEDGMENTS

The authors would like to acknowledge the Volkswagen Foundation (Grant No. 85391) (E.J.N., J.K.), PHOCUS (EU FET-Open Grant No. 240763) (D.V.S., J.K.), DST-Govt. of India (A.P.), and the Federal Ministry for Education and Research (BMBF) via the Potsdam Research Cluster for Georisk Analysis, Environmental Change and Sustainability (PROGRESS) (N.M.).

[1] H. Poincaré, Acta Mathematica **13**, 1 (1980).
[2] J. P. Eckmann, S. O. Kamphorst, and D. Ruelle, Euro. Phys. Lett. **4**, 973 (1987).
[3] N. Marwan, M. C. Romano, M. Thiel, and J. Kurths, Phys. Rep. **438**, 237 (2007), and references therein.
[4] N. Marwan, Eur. Phys. J. Spec. Top. **164**(1), 312 (2008).
[5] E. J. Ngamga, A. Nandi, R. Ramaswamy, M. C. Romano, M. Thiel, and J. Kurths, Phys. Rev. E **75**, 036222 (2007); E. J. Ngamga, A. Buscarino, M. Frasca, L. Fortuna, A. Prasad, and J. Kurths, Chaos **18**, 013128 (2008).
[6] J. B. Gao, Phys. Rev. Lett. **83**, 3178 (1999).
[7] J. B. Gao and H. Cai, Phys. Lett. A **270**, 75 (2000); J. B. Gao, Phys. Rev. E **63**, 066202 (2001); Phys. Lett. A **317**, 64 (2003).
[8] C. Grebogi, E. Ott, S. Pelikan, and J. A. Yorke, Physica D **13**, 261 (1984).
[9] U. Feudel, S. Kuznetsov and A. Pikovsky, *Strange Nonchaotic Attractors: Dynamics Between Order and Chaos in Quasiperiodically Forced Systems*, World Scientific Series on Nonlinear Science, Series A, Vol. 56 (World Scientific, Singapore, 2006).
[10] R. Benzi, G. Paladin, G. Parisi, and A. Vulpiani, J. Phys. A **18**, 2157 (1985).
[11] E. Aurell, G. Boffetta, A. Crisanti, G. Paladin, and A. Vulpiani, J. Phys. A **30**, 1 (1997); G. Paladin and A. Vulpiani, *ibid.* **19**, 1881 (1986).
[12] H. D. I. Abarbanel, R. Brown, and M. B. Kennel, J. Nonlinear Sci. **2**, 343 (1991).
[13] P. Grassberger, R. Badii, and A. Politi, J. Stat. Phys. **51**, 135 (1988).
[14] E. Ott, *Chaos in Dynamical Systems* (Cambridge University Press, Cambridge, 1994).
[15] H. Fujisaka, Prog. Theor. Phys. **70**, 1264 (1983).
[16] A. Prasad and R. Ramaswamy, Phys. Rev. E **60**, 2761 (1999).
[17] A. Prasad, V. Mehra, and R. Ramaswamy, Phys. Rev. E **57**, 1576 (1998).
[18] A. Prasad, V. Mehra, and R. Ramaswamy, Phys. Rev. Lett. **79**, 4127 (1997); A. Prasad, S. S. Negi, and R. Ramaswamy, Int. J. Bifurcation Chaos **11**, 291 (2001); A. Prasad, A. Nandi, and R. Ramaswamy, *ibid.* **17**, 3397 (2007).
[19] J. B. Gao, J. Hu, W. W. Tung, and Y. H. Cao, Phys. Rev. E **74**, 066204 (2006); J. Hu, J. B. Gao, and W. W. Tung, Chaos **19**, 028506 (2009).
[20] J. F. Heagy and S. M. Hammel, Physica D **70**, 140 (1994).
[21] T. Nishikawa and K. Kaneko, Phys. Rev. E **54**, 6114 (1996).
[22] A. Bondeson, E. Ott, and T. M. Antonsen Jr., Phys. Rev. Lett. **55**, 2103 (1985).
[23] S. Schinkel, O. Dimigen, and N. Marwan, Eur. Phys. J. Spec. Top. **164**, 45 (2008).
[24] G. M. Mindlin and R. Gilmore, Physica D **58**, 229 (1992); M. Koebbe and G. Mayer-Kress, in *Proceedings of SFI Studies in the Science of Complexity*, Vol. XXI (Addison-Wesley, Reading, MA, 1992), p. 361; J. P. Zbilut and C. L. Webber Jr., Phys. Lett. A **171**, 199 (1992).
[25] H. D. I. Abarbanel, R. Brown, and M. B. Kennel, J. Nonlinear Sci. **1**, 175 (1991).
[26] This theorem states conditions under which the mean of a sufficiently large number of independent random variables, each with finite mean and variance, will be approximately normally distributed.
[27] Y. Pomeau and P. Manneville, Commun. Math. Phys. **74**, 189 (1980).
[28] A. Venkatesan, M. Lakshmanan, A. Prasad, and R. Ramaswamy, Phys. Rev. E **61**, 3641 (2000).
[29] D. V. Senthilkumar, K. Srinivasan, K. Thamilmaran, and M. Lakshmanan, Phys. Rev. E **78**, 066211 (2008); K. Srinivasan, D. V. Senthilkumar, R. Suresh, K. Thamilmaran, and M. Lakshmanan, Int. J. Bifurcation Chaos **19**, 4131 (2009).
[30] W. L. Ditto, S. Rauseo, R. Cawley, C. Grebogi, G. H. Hsu, E. Kostelich, E. Ott, H. T. Savage, R. Segnan, M. L. Spano, and

J. A. Yorke, Phys. Rev. Lett. **63**, 923 (1989); H. T. Savage, W. L. Ditto, P. A. Braza, M. L. Spano, and W. C. Spring, J. Appl. Phys. **67**, 5619 (1990); H. T. Savage and M. L. Spano, *ibid*. **53**, 8002 (1982); H. T. Savage and C. Adler, J. Magn. Magn. Mater. **58**, 320 (1986); M. Lakshmanan and K. Murali, *Chaos in Nonlinear Oscillators: Synchronization and Controlling* (World Scientific, Singapore, 1996).

[31] W. L. Ditto, M. L. Spano, H. T. Savage, S. N. Rauseo, J. Heagy, and E. Ott, Phys. Rev. Lett. **65**, 533 (1990).

[32] A. Facchini and H. Kantz, Phys. Rev. E **75**, 036215 (2007).

[33] F. J. Romeiras and E. Ott, Phys. Rev. A **35**, 4404 (1987).

[34] F. J. Romeiras, A. Bondeson, E. Ott, T. M. Andonsen Jr., and C. Grebogi, Physica D **26**, 277 (1987).

[35] M. Ding, C. Grebogi, and E. Ott, Phys. Rev. A **39**, 2593 (1989).

[36] G. Ruiz and P. Parmananda, Phys. Lett. A **367**, 478 (2007).